PHYSICAL ASPECTS OF RAREFIED HYPERSONIC WEDGE FLOW

Wilson F. N. Santos
National Institute for Space Research
Combustion and Propulsion Laboratory
12630-000 Cachoeira Paulista, SP, Brazil
wilson@lcp.inpe.br

Abstract. *This paper presents numerical simulations of truncated wedges in rarefied hypersonic flow. The work is motivated by the interest in investigating the effect of the frontal-face thickness on the aerodynamic surface quantities on the wedges. The impact of the geometric bluntness, dictated by heating, handling or manufacturing requirements, on the aerodynamic heating has been investigated by employing the Direct Simulation Monte Carlo (DSMC) method. The bluntness investigated resulted on significant departures from ideal aerodynamic performance of hypersonic configurations such as waveriders. The results presented highlight the sensitivity of the heat transfer coefficient to changes on the frontal-face thickness of the leading edges. Some significant differences on the heat transfer coefficient provided by the DSMC method and by the free molecular flow equation were noted along the body surface at the vicinity of the frontal-face/afterbody junction for the leading edges with thickness Knudsen number of 100, 10 and 1. It was found that the heat transfer rate for the smallest frontal-face thickness approached the free molecular limit from above whereas that obtained for the largest frontal-face thickness approached from below. According to the results, for the conditions on the investigation, there is a particular frontal-face thickness that represents the crossover point where the approach to the free molecular limit is at the level of the free molecular limit.*

Keywords*: Hypersonic Flow, Rarefied Flow, DSMC, Wedge, Free Molecular Flow.*

1. INTRODUCTION

In typical aerospace mission, vehicle performance is directly related to the aerodynamic characteristics of the design. In particular, the lift-to-drag (L/D) ratio indicates one aspect of the aerodynamic efficiency of the vehicle. One class of aerospace vehicles that have shown the ability to attain a higher L/D ratio compared to conventional vehicle designs is waveriders. Waverider configurations, introduced by Nonweiler (1959), are derived from a known analytical flowfield, such as flow over a two-dimensional wedge or flow around a slender cone. These configurations are designed analytically with infinitely sharp leading edges for shock wave attachment. The attached shock wave eliminates flow leakage from the high-pressure lower surface to the upper surface, resulting in the potential for a high L/D ratio.

Usually, it is extremely difficult to construct a perfectly sharp leading edge. Any manufacturing error may result in a significant deviation from the design contour. In addition to that, sharp leading edges are associated to high aerodynamic heating since the heat flux to the leading edge varies inversely with the leading-edge radius. Therefore, for either heat transfer or manufacturing concerns, hypersonic leading edge should be blunt. However, blunt leading edge promotes shock-wave detachment, making leading-edge blunting a major concern in the design and prediction of flowfields of hypersonic waverider configurations.

In this scenario, Santos (2002 and 2005) investigated the effect of the frontal-face thickness on the flowfield structure and on the aerodynamic surface quantities over truncated wedges. The emphasis of the works was to provide a critical analysis on maximum allowable geometric bluntness, dictated by either heat transfer or manufacturing requirements, resulting on reduced departures from ideal aerodynamic performance of the hypersonic vehicle. Thus, allowing the blunted leading edge to more closely represents the original sharp leading edge flowfield. The frontal-face thickness impact on the aerodynamic surface quantities was investigated for thickness defined by 0.01, 0.1 and 1 times the freestream mean free path, which correspond to thickness Knudsen number of 100, 10 and 1, respectively. Therefore, based on the frontal-face thickness, this Knudsen number range covers from the transitional flow regime to the free molecular flow one. Such analysis is also important when a comparison is to be made between experimental and theoretical results at the immediate vicinity of the leading edge, which generally assume a zero-thickness leading edge.

Santos (2003 and 2006) extended further the analysis presented by Santos (2002) on truncated wedges by performing a parametric study on these shapes with emphasis placed on the compressibility effects. The primary goal was to assess the sensitivity of the shock-wave standoff distance, stagnation point heating and total drag to changes on the freestream Mach number. The analysis showed that, for the thickness Knudsen number of 100, the heat transfer coefficient was above that predicted by the free molecular flow equations at the vicinity of the frontal-face/afterbody junction on the afterbody surface. In contrast, the heat transfer coefficient for thickness Knudsen number of 1 was below that predicted by the free molecular flow at the same station.

According to the literature (Pan and Probstein, 1965, Vidal and Bartz, 1965, Bird, 1966, McCroskey at al., 1966, McCroskey at al., 1967, Huang and Hartley, 1969, Huang and Hartley, 1970, Vogenitz and Takata, 1971, Huang at al., 1973, Pullin and Harvey, 1976, and Dogra, 1989), this behavior has been observed on the aerodynamic surface

properties at the vicinity of the nose for sharp leading edges such as flat plate, wedge and cone. For the purpose of this introduction, it will be sufficient to describe only a few of these works.

Pan and Probstein (1965) investigated the aerodynamic surface quantities on flat plate by considering rarefied flow. Their solution showed that the heat-transfer rate could be greater than that predicted by the free-molecule value and that with decreasing Reynolds number the heat-transfer curve would approach the free-molecule value from above.

Vidal and Bartz (1965) observed from their experimental investigations on flat plates and wedges that the heat transfer rate approached the free molecular limit from above whereas those obtained at large wedge angles approached from below. According to them, for the particular conditions on the experiment, a 2-degree wedge angle appeared to be the crossover point where the approach to the free molecular limit was at the level of the free molecular limit. Their wedge flows were produced by pitching the flat-plate model to various compression angles.

In this scenario, the primary interest in the present account is to extend further the previous analysis on truncated wedges (Santos, 2006) by investigating closer the different behavior of the heat transfer coefficient, at the vicinity of the frontal-face/afterbody junction, when compared to that yielded by free molecular flow.

2. BODY SHAPE DEFINITION

The geometry of the leading edges in this work is the same as that presented in previous work (Santos 2006). The truncated wedges are modeled by assuming a sharp-edged wedge of half angle θ with a circular cylinder of radius R inscribed tangent to this sharp leading edge. The truncated wedges are also tangent to the sharp-edged wedge and the cylinder at the same common point. It was assumed a leading edge half angle of 10 degrees, a circular cylinder diameter of 10^{-2}m and frontal-face thickness t/λ_∞ of 0.01, 0.1 and 1, where λ_∞ is the freestream mean free path. Figure 1 illustrates schematically this construction.

It was assumed that the truncated wedges are infinitely long but only the length L is considered, since the wake region behind the truncated wedges is not of interest in the present investigation.

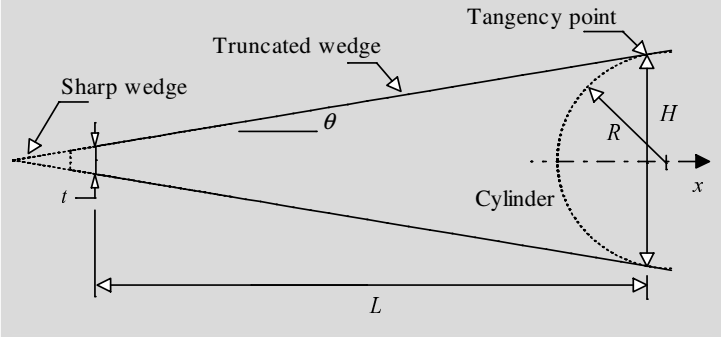

Figure 1: Drawing illustrating the leading edge shapes.

3. COMPUTATIONAL TOOL

The characteristic parameter that determines gas flow properties is the Knudsen number, $Kn = \lambda/l$, where λ is the molecular mean free path and l is the reference flow scale. In the continuum regime, as the Knudsen number tends toward zero, microscopic structure can be ignored, and a system can be completely described in terms of the macroscopic parameters such as velocity, density, pressure and temperature. In the free molecular regime, as the Knudsen number tends toward infinity, collisions between molecules can be neglected, and the flow behavior is by interactions between molecules and boundary surfaces. The region between the continuum and free-molecular regimes is called the transition regime. In the transition regime, where the microscopic structure can not be neglected, viscosity, heat conduction, relaxation, diffusion, and chemical processes are important. In this regime, the Knudsen number is of the order of unity.

The governing equation in the transition regime is the Boltzmann equation (Cercignani, 1988). It is a nonlinear integral-differential equation, closed with respect to the one-particle distribution function, which in turn determines the density of particles in a six-dimensional phase space of particle coordinates and velocities. In order to circumvent the difficult of a direct solution of the Boltzmann equation, the Direct Simulation Monte Carlo (DSMC) method has been the approach of choice for the study of complex multidimensional flows of rarefied hypersonic aerothermodynamics.

The DSMC method (Bird, 1994) model a gas flow by using a computer to track the trajectory of simulated particles, where each simulated particle represents a fixed number of real gas particles. The simulated particles are allowed to move and collide, while the computer stores their position coordinates, velocities and other physical properties such as internal energy. Figure 2(a) illustrates the DSMC Algorithm.

Collisions in the present DSMC code are modeled by the variable hard sphere (VHS) molecular model (Bird, 1981) and the no time counter (NTC) collision sampling technique (Bird, 1989). The Borgnakke-Larsen statistical model (Borgnakke and Larsen, 1975) is used to repartition energy among the internal and translation modes after a collision. Simulations are performed using a non-reacting gas model consisting of two chemical species, N_2 and O_2. The vibrational temperature is controlled by the distribution of energy between the translational and rotational modes after an inelastic collision. The rates of rotational and vibrational relaxation are dictated by collision numbers Z_R and Z_V, respectively. The collision numbers are traditionally given as constants, 5 for rotation and 50 for vibration.

For the numerical treatment of the problem, the flowfield around the leading edges is divided into an arbitrary number of regions, which are subdivided into computational cells. The cells are further subdivided into subcells, two subcells/cell in each coordinate direction. The cell provides a convenient reference for the sampling of the macroscopic gas properties, while the collision partners are selected from the same subcell for the establishment of the collision rate.

The computational domain used for the calculation is made large enough so that body disturbances do not reach the upstream and side boundaries, where freestream conditions are specified. A schematic view of the computational domain is depicted in Fig. 2(b).

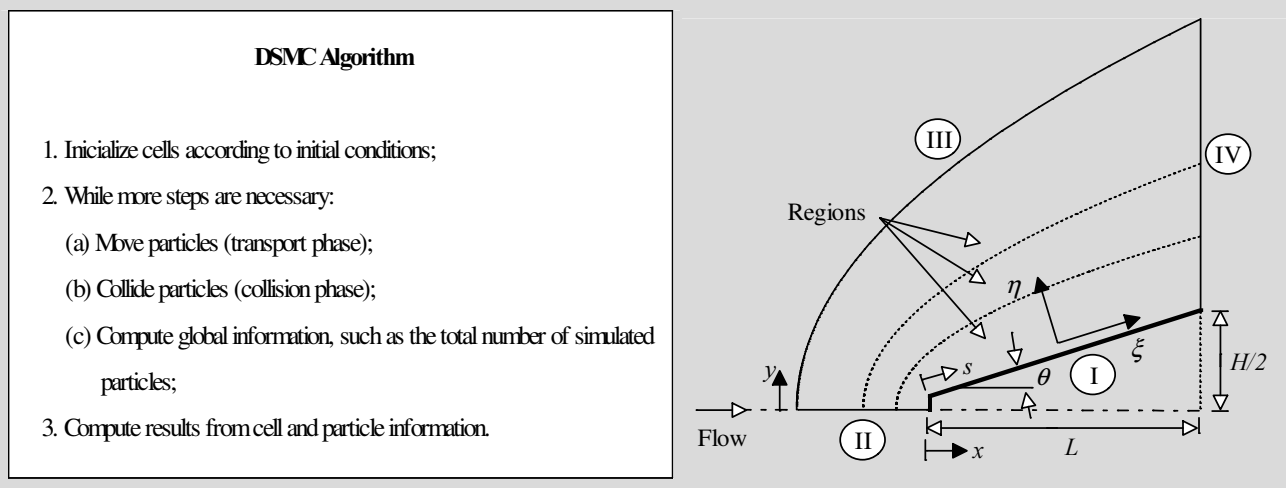

Figure 2: (a) The DSMC algorithm and (b) the computational domain.

Referring to Fig. 2(b), side I is defined by the body surface. Diffuse reflection with complete thermal accommodation is the condition applied to this side. In a diffuse reflection, the molecules are reflected equally in all directions, and the final velocity of the molecules is randomly assigned according to a half-range Maxwellian distribution determined by the wall temperature. Advantage of the flow symmetry is taken into account, and molecular simulation is applied to one-half of a full configuration. Thus, side II is a plane of symmetry, where all flow gradients normal to the plane are zero. At the molecular level, this plane is equivalent to a specular reflecting boundary. Side III is the freestream side through which simulated molecules enter and exit. Finally, the flow at the downstream outflow boundary, side IV, is predominantly supersonic and vacuum condition is specified (Bird, 1994). At this boundary, simulated molecules can only exit.

The numerical accuracy in DSMC method depends on the cell size chosen, on the time step as well as on the number of particles per computational cell. In the DSMC code, the linear dimensions of the cells should be small in comparison with the scale length of the macroscopic flow gradients normal to streamwise directions, which means that the cell dimensions should be of the order of or smaller than the local mean free path (Alexander et al., 1998, Alexander et al., 2000). The time step should be chosen to be sufficiently small in comparison with the local mean collision time (Garcia and Wagner, 2000, and Hadjiconstantinou, 2000). In general, the total simulation time, discretized into time steps, is identified with the physical time of the real flow. Finally, the number of simulated particles has to be large enough to make statistical correlations between particles insignificant.

These effects were investigated in order to determine the number of cells and the number of particles required to achieve grid independence solutions. Grid independence was tested by running the calculations with half and double the number of cells in ξ and η directions (see Fig. 2(b)) compared to a standard grid. Solutions (not shown) were near identical for all grids used and were considered fully grid independent. A discussion of these effects on the aerodynamic surface quantities is described in details in Santos (2006).

4. COMPUTATIONAL PROCEDURE

The flowfield properties upstream and adjacent to the leading edge of a body are affected by molecules reflected from the edge region. The degree of the effect is in part conditioned by the edge geometry. In an effort to understand the behavior of the aerodynamic surface properties at the vicinity of the leading-edge nose, the present account will employ a procedure based on the physics of the particles. In this respect, the flowfield is assumed to consist of three distinct classes of molecules: those molecules from the freestream that have not been affected by the presence of the leading edge are denoted as class I molecules; those molecules that, at some time in their past history, have struck and been reflected from the body surface are denoted as class II molecules; and finally, those molecules that have been indirectly

affected by the presence of the body are defined as class III molecules. Figure 3 illustrates the definition for the molecular classes.

It is assumed that the class I molecule changes to class III molecule when it collides with class II or class III molecule. Class I or class III molecule is progressively transformed into class II molecule when it interacts with the body surface. Also, a class II molecule remains class II regardless of subsequent collisions and interactions. Hence, the transition from class I molecules to class III molecules may represent the shock wave, and the transition from class III to class II may define the boundary layer.

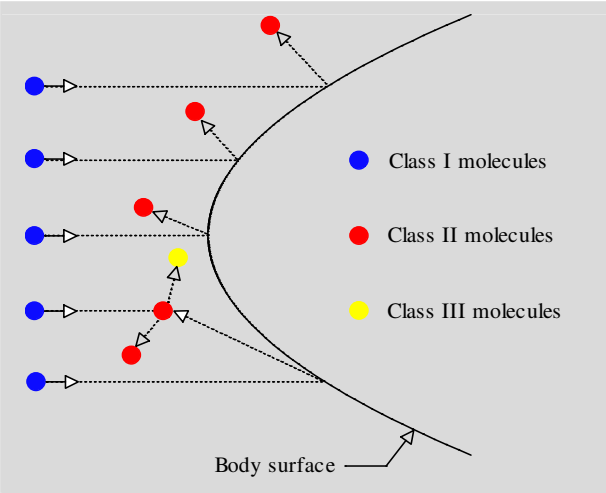

Figure 3: The molecular class definition.

5. FREESTREAM AND FLOW CONDITIONS

The freestream and flow conditions used in the present calculations are those given by Santos (2006) and summarized in Tab. 1. In addition, the gas properties (Bird, 1994) are tabulated in Tab. 2. The freestream velocity V_∞ was assumed to be constant at 1.49, 2.38 and 3.56 km/s, which correspond to freestream Mach number M_∞ of 5, 8, and 12, respectively. The translational and vibrational temperatures in the freestream are in equilibrium at 220 K, and the leading edge surface has a constant temperature T_w of 880 K for all cases considered.

Table 1: Freestream Conditions

Temperature T_∞ (K)	Pressure p_∞ (N/m^2)	Density ρ_∞ (kg/m^3)	Number density n_∞ (m^{-3})	Viscosity μ_∞ (Ns/m^2)	Mean free path λ_∞ (m)
220.0	5.582	8.753×10^{-5}	1.8209×10^{21}	1.455×10^{-5}	9.03×10^{-4}

Table 2: Gas Properties

	Mole fraction X	Molecular mass m (kg)	Molecular diameter d (m)	Viscosity index ω
O_2	0.237	5.312×10^{-26}	4.01×10^{-10}	0.77
N_2	0.763	4.65×10^{-26}	4.11×10^{-10}	0.74

The overall Knudsen number Kn_t, defined as the ratio of the freestream mean free path λ_∞ to the leading edge thickness t, corresponds to 100, 10 and 1 for leading edge thickness t/λ_∞ of 0.01, 0.1 and 1, respectively. The Reynolds number Re_t covers the range from 0.193 to 19.3, based on conditions in the undisturbed stream with leading edge thickness t as the characteristic length.

6. COMPUTATIONAL RESULTS AND DISCUSSION

The purpose of this section is to discuss differences in the heat transfer coefficient due to variations on the leading-edge thickness and to compare with that by considering free molecular flow. In order to present the problem coherently it is necessary to repeat the analysis of previous publication to some extent. In doing so the present approach begins with the results of Santos (2006), in which, for any particular reasons, the heat transfer coefficient was above that predicted by the free molecular flow equations.

The heat transfer coefficient C_h is defined as being,

$$C_h = \frac{q_w}{\frac{1}{2}\rho_\infty V_\infty^3} \tag{1}$$

where the heat flux q_w to the body surface is calculated by the net energy fluxes of the molecules impinging on the surface. A flux is regarded as positive if it is directed toward the surface. The heat flux q_w is related to the sum of the translational, rotational and vibrational energies of both incident and reflected molecules as defined by,

$$q_w = q_i + q_r = \sum_{j=1}^{N} \left\{ \left[\frac{1}{2} m_j c_j^2 + e_{Rj} + e_{Vj} \right]_i + \left[\frac{1}{2} m_j c_j^2 + e_{Rj} + e_{Vj} \right]_r \right\} \tag{2}$$

where N is the number of molecules colliding with the surface by unit time and unit area, m is the mass of the molecules, c is the velocity of the molecules, e_R and e_V stand for the rotational and vibrational energies, and subscripts i and r refer to incident and reflected molecules.

Distributions of the heat transfer coefficient C_h along the frontal and afterbody surfaces are illustrated in Figs. 4 and 5, respectively, parameterized by the freestream Mach number for leading-edge thickness t/λ_∞ of 0.01, 0.1 and 1, which correspond to thickness Knudsen number Kn_t of 100, 10 and 1, respectively. In this set of plots, Figs. 4(a-c) correspond to the heat transfer coefficient C_h to the frontal face as a function of the dimensionless height Y ($\equiv y/\lambda_\infty$), measured from the stagnation point up to the shoulder of the wedge, and Figs. 5(a-c) correspond to the heat transfer coefficient C_h to the afterbody surface of the wedge as a function of the dimensionless arc length S ($\equiv s/\lambda_\infty$), measured from the shoulder of the leading edge. For purpose of comparison, Figs. 4 and 5 display the free molecular flow (FM) limit value for the heat transfer coefficient by assuming collisionless flow (Bird, 1994).

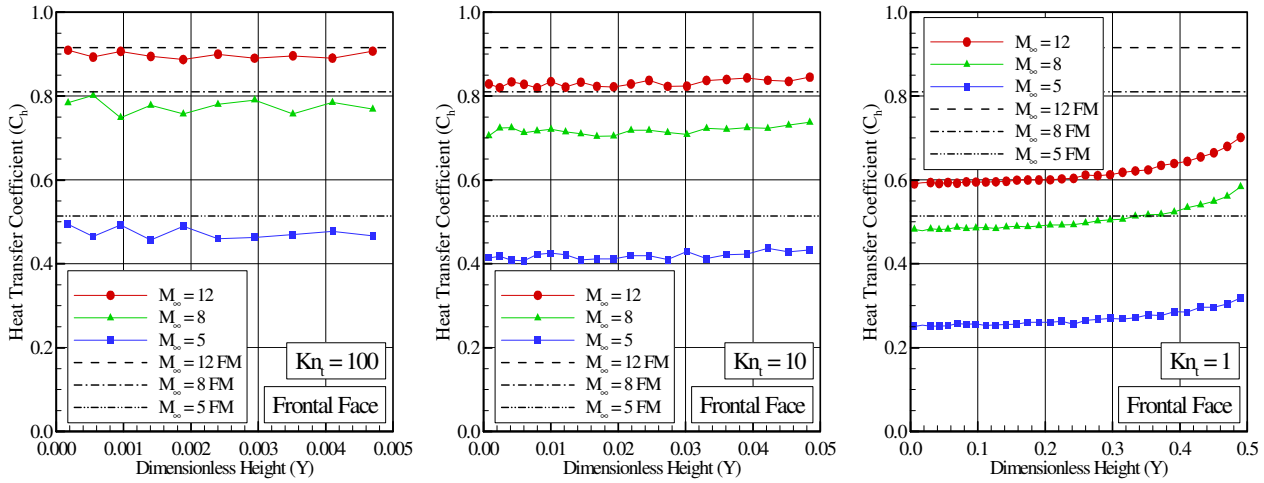

Figure 4: Distributions of the heat transfer coefficient C_h along the frontal surface of the leading edge as a function of the freestream Mach number for thickness Knudsen number Kn_t of (a) 100, (b) 10 and (c) 1.

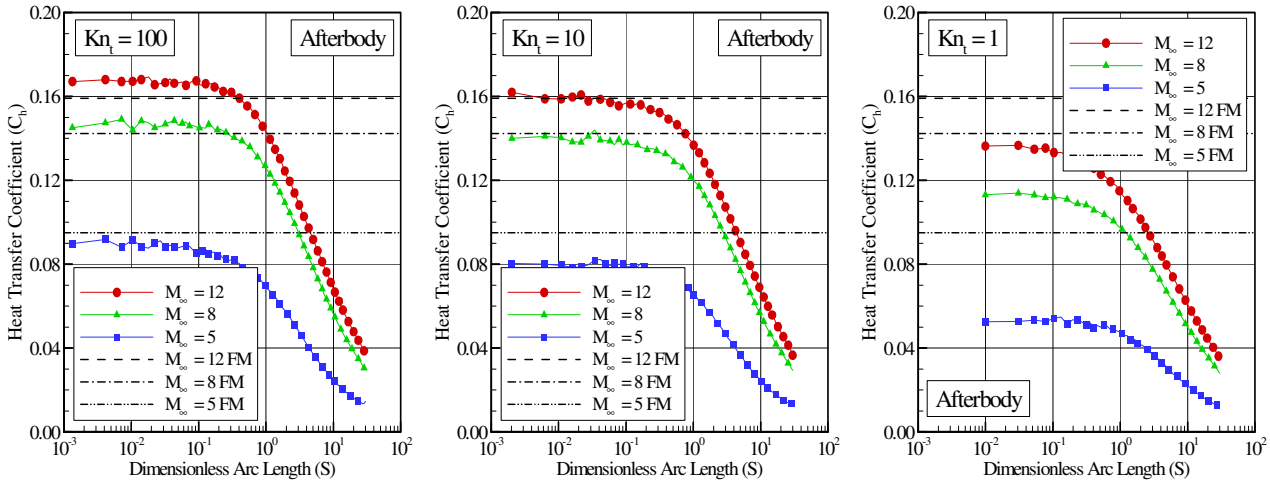

Figure 5: Distributions of the heat transfer coefficient C_h along the afterbody surface of the leading edge as a function of the freestream Mach number for thickness Knudsen number Kn_t of (a) 100, (b) 10 and (c) 1.

Free-molecular flow or collisionless flow is the limiting case in which the Knudsen number tends to infinity. It is the subdivision of rarefied gas dynamics corresponding to the lowest densities, therefore with very high mean free paths, or with very small characteristic dimensions. Analytical expressions for number density of the gas just above the surface, number flux, pressure coefficient, heat transfer coefficient and skin friction coefficient have been derived (Bird, 1994)

by assuming that the flow past the surface element is in Maxwellian equilibrium with freestream number density n_∞, temperature T_∞, macroscopic velocity V_∞ inclined at an angle of incidence α to the unit normal vector to the surface element, and diffuse reflection. However, the body slope angle θ is related to the angle of incidence α of the element surface by $\pi/2$-α, and it seems to be more appropriate for this work. In this fashion, the heat transfer coefficient by considering free molecular flow is given by the following expression,

$$C_h = \frac{1}{2\sqrt{\pi}\beta_\infty^3}\left\{\left[\beta_\infty^2 + \frac{\gamma}{\gamma-1} - \frac{\gamma+1}{2(\gamma-1)}\frac{T_w}{T_\infty}\right]\left[\exp(-\chi^2) + \sqrt{\pi}\chi(1+erf\chi)\right] - \frac{1}{2}\exp(-\chi^2)\right\} \tag{3}$$

where γ is the specific heat ratio, β_∞ is the speed ratio of the freestream defined by $V_\infty\sqrt{2RT_\infty}$ and $\chi = \beta_\infty sin\theta$ with R standing for the gas constant.

By considering free molecular flow, the heat transfer coefficient C_h on the frontal surface predicted by Eq. (3) is 0.514, 0.810 and 0.916 for freestream Mach number M_∞ of 5, 8 and 12, respectively. For the afterbody surface, the FM values are 0.095, 0.142 and 0.159 for M_∞ of 5, 8 and 12, respectively.

According to Figs. 4 and 5, it is seen that the heat transfer coefficient C_h changes on the frontal and afterbody surfaces of the wedge with increasing not only the freestream Mach number but also the frontal-face thickness. As the freestream Mach number increases from 5 to 12, the kinetic energy of the freestream molecules increases. Consequently, the heat flux to the body surface increases. An understanding of this behavior can be gained by analyzing Eq. (2). The incident component of the velocity c of the molecules is a function of the freestream Mach number. However, the reflected component of the molecular velocity is not a function of the freestream Mach number. Due to the diffuse reflection model, the reflected component of the molecular velocity is obtained from a Maxwellian distribution that only takes into account for the temperature of the body surface, which has the same value for the freestream Mach number range investigated. It should also be emphasized that the number of molecules colliding with the surface by unit time and unit area, N, which appears in Eq. (2), is the same for the incident and reflected components of the heat transfer coefficient C_h. Nevertheless, N increases on the frontal and afterbody surfaces of the leading edges with increasing the freestream Mach number and the frontal-face thickness, as will be seen subsequently. Particular attention is paid to the heat transfer coefficient at the vicinity of the shoulder for the bluntest case investigated, $Kn_t = 1$ ($t/\lambda_\infty = 1$). For the $Kn_t = 1$ case, the heat transfer coefficient C_h increases at the vicinity of the shoulder, in contrast to the aerodynamically sharp leading edge cases investigated, $Kn_t = 10$ and 100. This behavior would be also expected since the velocity of the molecules increases at the vicinity of the shoulder, where the flow is allowed to expand. In addition, the contribution of the translational energy to the net heat flux varies with the square of the velocity of the molecules, as shown in Eq. (2).

Referring to Fig. 5(a), it is very encouraging to observe that the heat transfer coefficient C_h on the afterbody surface, at the vicinity of the flat-face/afterbody junction, is above that predicted by the free molecular flow equations. It should be mentioned in this context that this behavior has been observed on the surface properties at the vicinity of the nose for sharp leading edges such as flat plate, wedge and cone. As an illustrative example, Vidal and Bartz (1965) observed from their experimental investigations on flat plates and wedges that the heat transfer rate approached the free molecular limit from above whereas those obtained at large wedge angles approached from below. According to them, for the particular conditions on the experiment, a 2-degree wedge angle appeared to be the crossover point where the approach to the free molecular limit was at the level of the free molecular limit. Their wedge flows were produced by pitching the flat-plate model to various compression angles.

With this perspective in mind, Fig. 5 reveals the presence of two possible "crossover points". The first one is related to the freestream Mach number effect on the thickness Knudsen number Kn_t of 100 illustrated in Fig. 5(a). It is clearly seen that, for freestream Mach number of 12 and 8, the heat transfer coefficient C_h approaches from above. Conversely, for freestream Mach number of 5, C_h approaches from below. The second one is connected to the frontal-face thickness effect for freestream Mach number of 8 and 12. For thickness Knudsen number Kn_t of 100, Fig. 5(a), the heat transfer coefficient C_h approaches from above, and for thickness Knudsen number Kn_t of 1, C_h approaches from below, as shown in Fig. 5(c). Based on Vidal and Bartz (1965), for the first case, the crossover point is between freestream Mach number of 8 and 5. For the second case, the leading edge defined by thickness Knudsen number Kn_t of 10 appears to be the crossover point where the approach to the free molecular limit is at the level of the free molecular limit.

This behavior is explained by the fact that collision of the oncoming freestream molecules (class I molecules), therefore high-velocity molecules, with the molecules emitted from the body surface (class II molecules) will on the average causes at least some of the oncoming molecules to be reflected onto the body surface, thereby increasing the heat transfer rate over the free molecular value owing to the increased energy. This result is in contrast to the rarefied flow past blunt leading edge, Kn_t of 1 as shown in Fig. 5(c). For the blunt leading edge, the effect of collisions of the oncoming freestream molecules with those emitted from the surface will be to deflect some of the incident molecules from the surface, thereby reducing the heat transfer rate relative to the free molecular value.

In what follows, it proves helpful to present the number flux to the body surface. The number flux N is calculated by sampling the molecules impinging on the surface by unit time and unit area. The impact of the number flux on the

frontal and afterbody surfaces due to variations on the frontal-face thickness is demonstrated in Figs. 6 and 7, respectively, for thickness Knudsen number Kn_t of 100, 10 and 1. In this set of plots, the dimensionless number flux N_f stands for the number flux N normalized by $n_\infty V_\infty$, where n_∞ is the freestream number density and V_∞ is the freestream velocity.

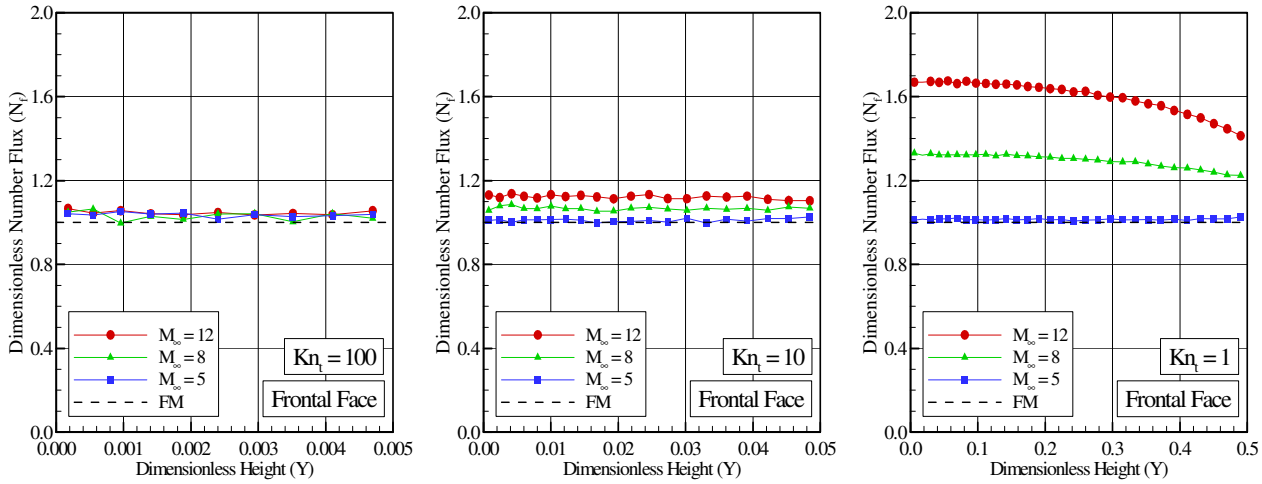

Figure 6: Distributions of the dimensionless number flux N_f along the frontal surface of the leading edge as a function of the freestream Mach number for thickness Knudsen number Kn_t of (a) 100, (b) 10 and (c) 1.

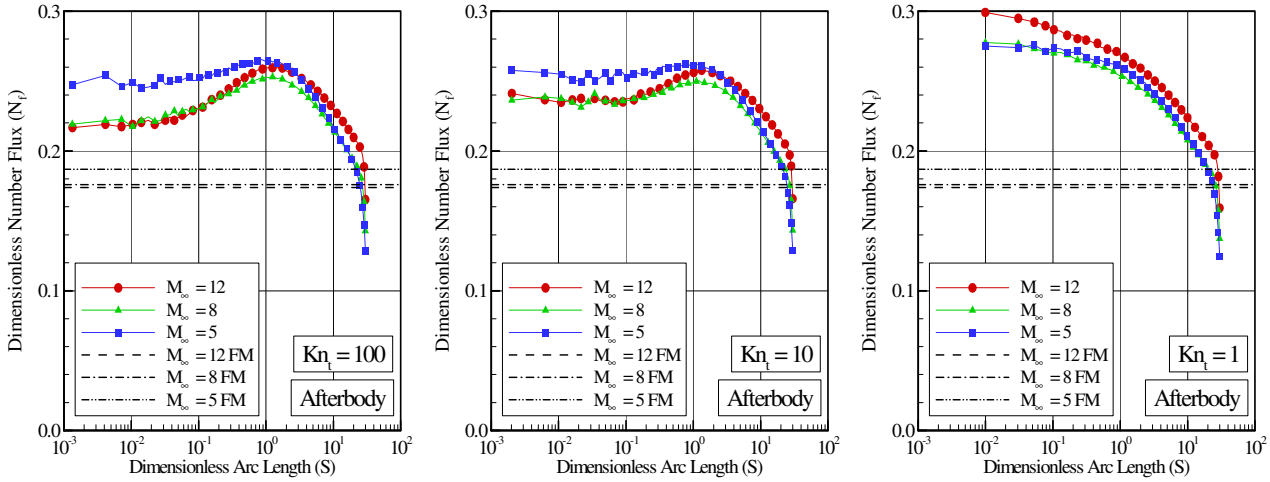

Figure 7: Distributions of the dimensionless number flux N_f along the afterbody surface of the leading edge as a function of the freestream Mach number for thickness Knudsen number Kn_t of (a) 100, (b) 10 and (c) 1.

For completeness, Figs. 6 and 7 display the free molecular flow (FM) limit value for the dimensionless number flux by assuming collisionless flow. In this fashion, the dimensionless number flux by considering free molecular flow is given by the following expression (Bird, 1994),

$$\frac{N}{n_\infty V_\infty} = \frac{1}{2\sqrt{\pi}\beta_\infty}\left[\exp(-\chi^2) + \sqrt{\pi}\chi(1+erf\chi)\right] \tag{4}$$

where β_∞ is the speed ratio of the freestream defined by $V_\infty\sqrt{2RT_\infty}$ and $\chi = \beta_\infty sin\theta$ with R standing for the gas constant.

By analyzing Eq. (4), the dimensionless number flux for free molecular flow tends to $sin\theta$ as the freestream speed ratio $\beta_\infty \to \infty$. As the freestream Mach number increases from 5 to 12, the freestream speed ratio β_∞ increases from 4.18 to 9.44. For the frontal surface, with a slope angle θ of 90 degrees, $N_f\,(\equiv N/n_\infty V_\infty) = 1$ for freestream Mach number of 5, 8, and 12. As a result, the dimensionless number flux for free molecular flow becomes independent of the freestream speed ratio or freestream Mach number for the range investigated. This is related to the Mach number independence principle. For the afterbody surface, with a slope angle of 10 degrees, the free molecular value from Eq, (4) is 0.187,

0.176 and 0.174 for freestream Mach number of 5, 8 and 12, respectively.

By looking first at Figs. 6(a-c), it is clearly seen that, the dimensionless number flux to the frontal surface increases by increasing the frontal-face thickness. This is an expected behavior since the leading edge changes aerodynamically from sharp to blunt with increasing the frontal-face thickness. In addition, for thickness Knudsen number Kn_t of 100, the dimensionless number flux N_f to the frontal surface approaches the limit value, $N/n_\infty V_\infty$, = 1, obtained by Eq. (4).

By turning next to Figs. 7(a-c), it is observed that the dimensionless number flux at the vicinity of the frontal-face/afterbody junction is far from the limit value predicted by the free molecular flow. It is also observed that the dimensionless number flux to the afterbody surface is one order of magnitude smaller than that to the frontal surface. Moreover, as mentioned earlier, as the frontal-face thickness increases, the leading edge becomes blunter and a rather different flow behavior is seen, as shown in Fig. 7(c), where the general shape for the number flux related to Kn_t = 1 displays a different profile as compared to those presented by the Kn_t = 10 and 100 cases.

By the time being, it proves helpful to add in this context that the free molecular flow equations are obtained from the premise that there are no intermolecular collisions. The fluxes of mass, momentum and energy incident to and reflected from a surface element can be treated separately and do not interfere with each other. The incident flux is entirely unaffected by the presence of the surface. In order to elucidate the effect posed above, in the sense that collision of the oncoming freestream molecules (class I) with the molecules emitted from the body surface (class II) will on the average causes at least some of the oncoming molecules to be reflected onto the body surface, thereby increasing the heat transfer rate over the free molecular value, the simulation for the leading edge represented by Kn_t = 100 is again examined for freestream Mach number of 8 and 12, but this time the intermolecular collisions will not be take into account in the simulation. This situation corresponds to skip the step 2(b) listed in the DSMC algorithm illustrated in Fig. 2(a).

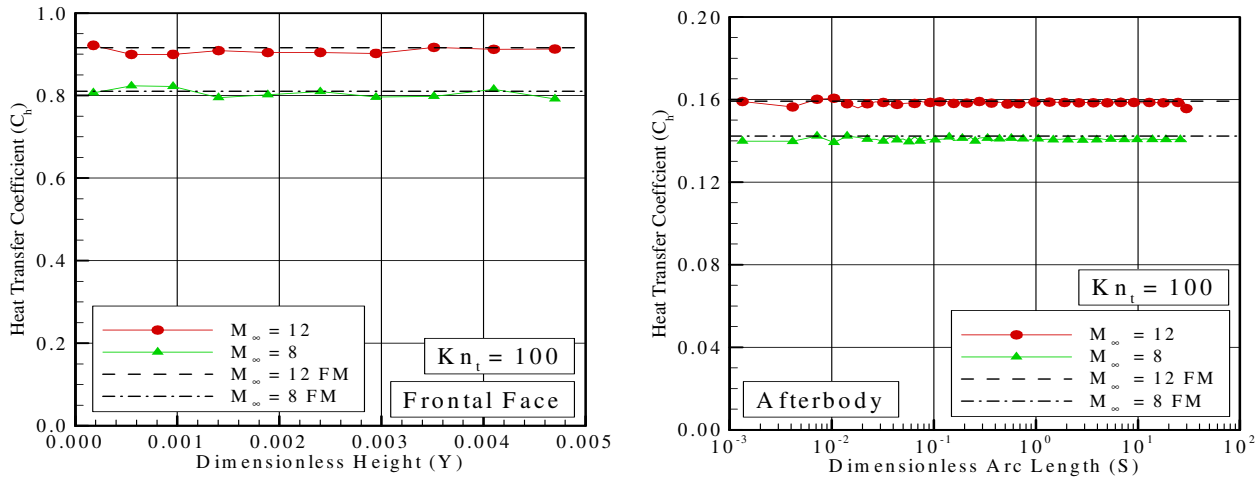

Figure 8: Distributions of heat transfer coefficient C_h along the (a) frontal and (b) afterbody surfaces of the leading edge as a function of the freestream Mach number for thickness Knudsen number Kn_t of 100.

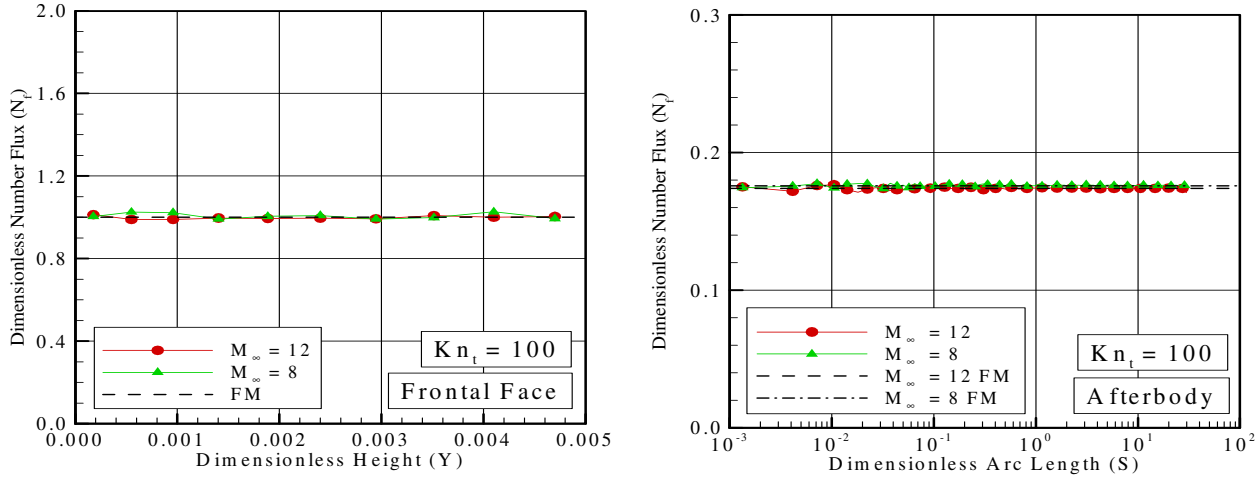

Figure 9: Distributions of the dimensionless number flux N_f along the (a) frontal and (b) afterbody surfaces of the leading edge as a function of the freestream Mach number for thickness Knudsen number Kn_t of 100.

In what follows, Figs. 8 and 9 compare the simulation results for the distributions of heat transfer coefficient C_h and the dimensionless number flux N_f, respectively, by considering collisionless flow, with those yielded by the free molecular flow equations. As indeed is clear from these figures, the results obtained by the DSMC simulations are in excellent agreement with that yielded by the free molecular flow equations. It is thus firmly established that the heat transfer rate over the free molecular value, as shown in Fig. 5(a), is directly related to the collision of two groups of molecules: the oncoming freestream molecules (class I) and the molecules emitted from the body surface (class II).

At this point it is worth taking a closer look at the results from molecular class distributions. According to Fig. 3, the molecules are identified by class I, II and III. As the flowfield is divided into cells, information on collisions between the molecules may be stored, and interesting features can be drawn from the results. In this sense, for three classes of molecules, six pairs of collisions are possible: collisions of class I with class I, I versus II, I versus III, II versus II, II versus III and, finally, III versus III. Of particular interest in the present account are the collisions between molecules I versus II and II versus III in the cells adjacent to the body surface. In this fashion, Figs. 10 and 11 illustrate the distributions of class I versus class I and class II versus class III, respectively, for thickness Knudsen number Kn_t of 100, 10 and 1 with freestream Mach number of 12. In this set of figures, Y and X are the height y and length x, respectively, normalized by the freestream mean free path λ_∞. In addition, the contour scale represents the number of collisions for the specific pair of collisions divided by the total number of collisions inside the cell, after the establishment of the steady state.

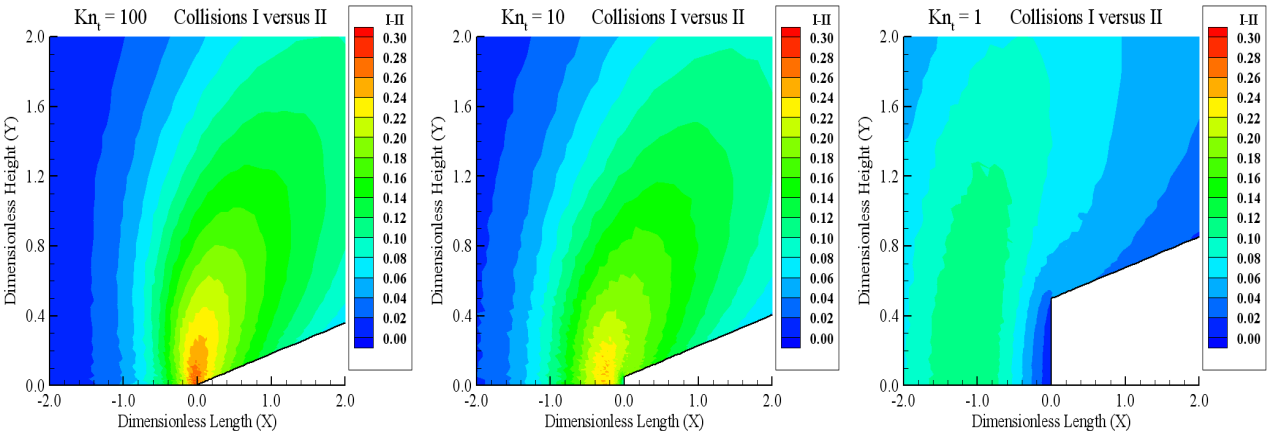

Figure 10: Distributions of collisions between molecules of class I with class II at the vicinity of the leading edges for thickness Knudsen number Kn_t of (a) 100, (b) 10 and (c) 1, and freestream Mach number of 12.

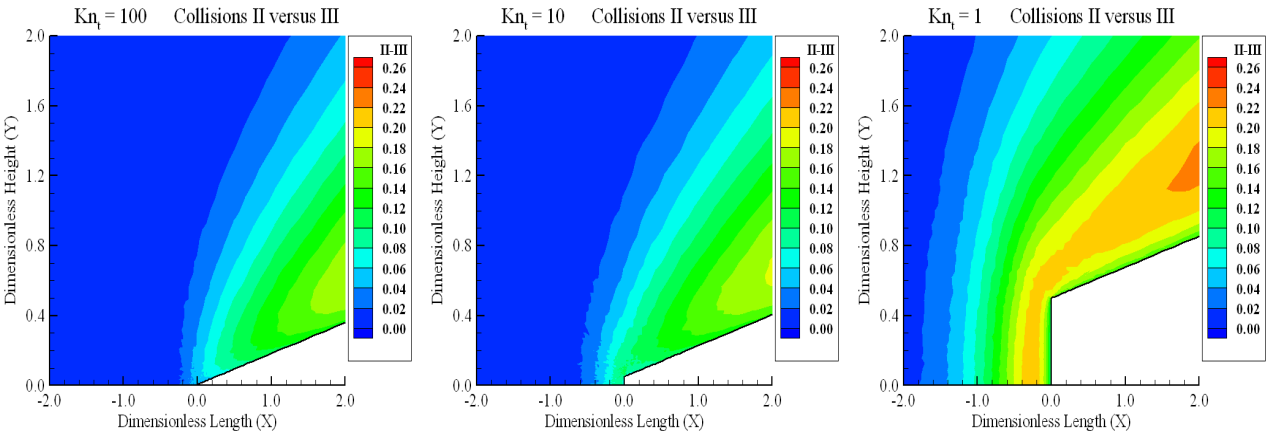

Figure 11: Distributions of collisions between molecules of class II with class III at the vicinity of the leading edges for thickness Knudsen number Kn_t of (a) 100, (b) 10 and (c) 1, and freestream Mach number of 12.

Looking first at Fig. 10(a), for the $Kn_t = 100$ case, it is clearly seen that collisions between molecules of class I with those of class II are responsible from 20% to 25% of the total number of collisions taking place in the cells adjacent to the afterbody surface along a distance of half freestream mean free path λ_∞, measured from the frontal-face/afterbody junction. Basically the distance where the heat transfer coefficient is above the free molecular limit as shown in Fig.

5(a). In contrast, for the Kn_t = 1 case, collisions class I versus class II contributes to only 5% of the total number of collisions, as illustrated in Fig. 10(c).

Turning next to Fig. 11(a), for the Kn_t = 100 case, it is observed that collisions between molecules of class II with those of class III represent around only 6% of the total number of collisions occurring adjacent to the afterbody surface at the vicinity of the frontal-face/afterbody junction. Conversely, for the Kn_t = 1 case, collisions class II versus class III contributes to around 15%, as depicted in Fig. 11(c).

5. CONCLUDING REMARKS

Numerical simulations of a rarefied hypersonic flow over truncated wedge have been performed by using the Direct Simulation Monte Carlo method. The simulations provided information concerning the nature of number flux and the heat transfer coefficient to the frontal and afterbody surfaces.

Compressibility effects and the frontal-face thickness impact on the number flux and on the heat transfer coefficient were investigated for a representative range of parameters. The freestream Mach number varied from 5 to 12. In addition to that, the frontal-face thickness ranged from 0.01 to 1 of the freestream mean free path, corresponding thickness Knudsen numbers from 100 to 1. Cases considered in this study covered the hypersonic flow from the transitional flow regime to the free molecular flow regime.

It was found that the heat transfer rate for the smallest frontal-face thickness case approached the free molecular limit from above whereas that obtained for the largest frontal-face thickness case approached from below. According to the results, for the conditions on the investigation, there is a particular frontal-face thickness that represents the crossover point where the approach to the free molecular limit is at the level of the free molecular limit.

The analysis also showed that for the smallest frontal-face thickness case, the heat transfer coefficient approached the free molecular limit from above for freestream Mach number of 12. Nevertheless, for freestream Mach number of 5, the heat transfer coefficient approached from below. As a result, there is a particular freestream Mach number that represents the crossover point where the approach to the free molecular limit is at the level of the free molecular limit.

7. REFERENCES

Alexander, F. J., Garcia, A. L., and, Alder, B. J., 1998, "Cell Size Dependence of Transport Coefficient in Stochastic Particle Algorithms", Physics of Fluids, Vol. 10, No. 6, pp. 1540-1542.

Alexander, F. J., Garcia, A. L., and, Alder, B. J., 2000, "Erratum: Cell Size Dependence of Transport Coefficient is Stochastic Particle Algorithms", Physics of Fluids, Vol. 12, No. 3, pp. 731-731.

Bird, G. A., 1966, "Aerodynamic Properties of Some Simple Bodies in the Hypersonic Transition Regime", *AIAA Journal*, vol. 4, No. 1, pp. 55-60.

Bird, G. A., 1981, "Monte Carlo Simulation in an Engineering Context", Progress in Astronautics and Aeronautics: Rarefied gas Dynamics, Ed. Sam S. Fisher, Vol. 74, part I, AIAA New York, pp. 239-255.

Bird, G. A., 1989, "Perception of Numerical Method in Rarefied Gasdynamics", Rarefied gas Dynamics: Theoretical and Computational Techniques, Eds. E. P. Muntz, and D. P. Weaver and D. H. Capbell, Vol. 118, Progress in Astronautics and Aeronautics, AIAA, New York, pp. 374-395.

Bird, G. A., 1994, "Molecular Gas Dynamics and the Direct Simulation of Gas Flows", Oxford University Press, Oxford, England, UK.

Borgnakke, C. and Larsen, P. S., 1975, "Statistical Collision Model for Monte Carlo Simulation of Polyatomic Gas Mixture", Journal of Computational Physics, Vol. 18, No. 4, pp. 405-420.

Cercignani, C., 1988, "The Boltzmann Equation and Its Applications", Springer-Verlag, New York, NY.

Dogra, V. K., 1989, "Rarefied Flow Past a Flat Plate at Incidence", Rarefied Gas Dynamics: Theoretical and Computational Techniques, Progress in Astronautics and Aeronautics, Eds. E. P. Muntz, D. P. Weaver and D. H. Campbell, Vol. 118, pp. 567-581.

Garcia, A. L., and, Wagner, W., 2000, "Time Step Truncation Error in Direct Simulation Monte Carlo", Physics of Fluids, Vol. 12, No. 10, 2000, pp. 2621-2633.

Hadjiconstantinou, N. G., 2000, "Analysis of Discretization in the Direct Simulation Monte Carlo", Physics of Fluids, Vol. 12, No. 10, pp. 2634-2638.

Huang, A. B. and Hartley, D. L., 1969, "Kinetic Theory of the Sharp Leading Edge Problem in Supersonic Flow", The Physics of Fluids, Vol. 12, No. 1, pp. 96-108.

Huang, A. B. and Hartley, D. L., 1970, "Supersonic Leading Edge Problem According to the Ellipsoidal Model", The Physics of Fluids, Vol. 13, No. 2, pp. 309-317.

Huang, A. B., Hwang, P. F., Giddens, D. P. and Srinivasan, 1973, "High Speed Leading Edge Problem", The Physics of Fluids, Vol. 16, No. 6, pp. 814-824.

McCroskey, W. J., Bogdonoff, S. M. and McDougall, J. G., 1966, "An Experimental Model for the Sharp Flat Plate in Rarefied Hypersonic Flow", AIAA Journal, Vol. 4, No. 9, pp. 1580-1587.

McCroskey, W. J., Bogdonoff, S. M. and Genchi, A. P., 1967, "Leading Edge Flow Studies of Sharp Bodies in Rarefied Hypersonic Flow", Rarefied Gas Dynamics, Advance in Applied Mechanics, Suppl. 4, Vol. II, Academic Press, New York, pp. 467-486.

Nonweiler, T. R. F., 1959, "Aerodynamic Problems of Manned Space Vehicles", Journal of the Royal Aeronautical Society, Vol. 63, No. 589, pp. 521-528.

Pan, Y. S. and Probstein, R. F., 1965, "Rarefied-Flow Transition at a Leading Edge", in Fundamental Phenomena in Hypersonic Flow, Cornell University Press, Ithaca, NY, pp. 259-309.

Pullin, D. I. and Harvey, J. K., 1976, "A Numerical Simulation of the Rarefied Hypersonic Flat-Plate Problem", Journal of Fluid Mechanics, Vol. 78, part 4, pp. 689-707.

Santos, W. F. N., 2002, "Truncated Leading Edge Effects on Flowfield Structure of a Wedge in Low Density Hypersonic Flight Speed". Proceedings of the 9th Brazilian Congress of Thermal Engineering and Sciences (ENCIT 2002), Caxambu, MG, Brazil.

Santos, W. F. N., 2003, "Compressibility Effects on Flowfield Structure of Truncated Leading Edge in Low Density Hypersonic Flow". Proceedings of the 17th International Congress of Mechanical Engineering (COBEM 2003), São Paulo, SP, Brazil.

Santos, W. F. N., 2005, "Flat-Faced Leading-Edge Effects in Low-Density Hypersonic Wedge Flow", Journal of Spacecraft and Rockets, Vol. 42, No. 1, pp. 22-29.

Santos, W. F. N., 2006, "Effects of Compressibility on Aerodynamic Surface Quantities over Low-Density Hypersonic Wedge Flow". Journal of the Society of Mechanical Sciences and Engineering, Vol. 28, No. 3, pp. 311-321.

Vidal, R. J. and Bartz, J. A., 1965, "Experimental Studies of Low-Density Effects in Hypersonic Wedge Flows", Rarefied Gas Dynamics, Advance in Applied Mechanics, Suppl. 3, Vol. 1, Academic Press, New York, pp. 467-486.

Vogenitz, F. W. and Takata, G. Y., 1971, "Rarefied Hypersonic Flow about Cones and Flat Plates by Monte Carlo Simulation", AIAA Journal, Vol. 9, No. 1, pp. 94-100.